Atmospheric Research 186 (2017) 107–115

Contents lists available at ScienceDirect

Atmospheric Research

journal homepage: www.elsevier.com/locate/atmosres

Effects of cloud condensate vertical alignment on radiative transfer calculations in deep convective regions

Xiaocong Wang

State Key Laboratory of Numerical Modeling for Atmospheric Sciences and Geophysical Fluid Dynamics, Institute of Atmospheric Physics, Chinese Academy of Sciences, Beijing, China
Plateau Atmosphere and Environment Key Laboratory of Sichuan Province, Chengdu, China

ARTICLE INFO

Article history:
Received 8 August 2016
Received in revised form 30 October 2016
Accepted 22 November 2016
Available online 27 November 2016

Keywords:
Horizontal inhomogeneity
Topic:
Vertical alignment
Decorrelation length
Cloud radiative forcing
Stochastic ICA approach

ABSTRACT

Effects of cloud condensate vertical alignment on radiative transfer process were investigated using cloud resolving model explicit simulations, which provide a surrogate for subgrid cloud geometry. Diagnostic results showed that the decorrelation length L_{cw} varies in the vertical dimension, with larger L_{cw} occurring in convective clouds and smaller L_{cw} in cirrus clouds. A new parameterization of L_{cw} is proposed that takes into account such varying features and gives rise to improvements in simulations of cloud radiative forcing (CRF) and radiative heating, i.e., the peak of bias is respectively reduced by 8 W m^{-2} for SWCF and 2 W m^{-2} for LWCF in comparison with $L_{cw} =$ 1 km.

The role of L_{cw} in modulating CRFs is twofold. On the one hand, larger L_{cw} tends to increase the standard deviation of optical depth σ_τ, as dense and tenuous parts of the clouds would be increasingly aligned in the vertical dimension, thereby broadening the probability distribution. On the other hand, larger σ_τ causes a decrease in the solar albedo and thermal emissivity, as implied in their convex functions on τ. As a result, increasing (decreasing) L_{cw}leads to decreased (increased) CRFs, as revealed by comparisons among $L_{cw} = 0$, $L_{cw} = 1$ km and$L_{cw} = \infty$. It also affects the vertical structure of radiative flux and thus influences the radiative heating. A better representation of σ_τ in the vertical dimension yields an improved simulation of radiative heating. Although the importance of vertical alignment of cloud condensate is found to be less than that of cloud cover in regards to their impacts on CRFs, it still has enough of an effect on modulating the cloud radiative transfer process.

1. Introduction

Accurate parameterizations of clouds and their radiative properties are critical if numerical models are to produce realistic simulations of current climate or believable predictions of the future. Although this topic has received increased attention in recent decades (Lohmann et al., 1999; Bogenschutz and Krueger, 2013; Kuell and Bott, 2014), cloud representation in general circulation models (GCMs) is still in its infancy and contributes to one of the largest uncertainties in climate modeling (Bony and Dufresne, 2005). Apart from challenges in fractional cloudiness parameterization (Tompkins, 2002; Wang et al., 2015) and cloud cover overlap treatment (Wang et al., 2016), cloud representation is complicated by cloud hydrometeor inhomogeneity and associated vertical alignment.

Traditionally, GCMs represent clouds using grid-box means of a variable such as cloud liquid or ice water content (Zhang et al., 2013); however, this is far from realistic, as observed clouds exhibit dramatic variability at spatial scales smaller than the GCM grid (Tompkins, 2002). Remarkable errors can therefore occur in a series of physical processes, i.e., cloud autoconversion and radiative transfer (Pomroy and Illingworth, 2000; Larson et al., 2005). For instance, Cahalan et al. (1994a) found that the homogeneous assumption often yields overestimations in both shortwave and longwave cloud radiative forcings (CRFs). Pomroy and Illingworth (2000) obtained similar results and found the overestimation is essentially due to the non-linear relationship between cloud optical depth and solar albedo/thermal emissivity. There have been several attempts to remedy such biases. The simplest of these is to artificially scale down cloud optical depth. Cahalan et al. (1994a) suggested using a scaling factor of 0.7 based on maritime stratocumulus; however, they acknowledged the optimum value would vary in terms of time and location. Gu and Liou (2006) found that using a location-dependent inhomogeneity factor improved the global mean planetary albedo by 4%. Furthermore, Hill et al. (2012) proposed a parameterization of inhomogeneity that is suitable for inclusion in GCMs and obtained encouraging results. While the introduced inhomogeneity factor is beneficial in improving radiative budget simulations, it brings limited success in other aspects, i.e., radiative heating.

Another approach is the so-called stochastic independent column approximation (ICA), which generates subgrid-scale columns and allows each subcolumn to calculate radiative transfer independently (Cahalan et al., 1994b; Barker et al., 1999). The accuracy of this method

E-mail address: wangxc@lasg.iap.ac.cn.

http://dx.doi.org/10.1016/j.atmosres.2016.11.014

depends on how closely the generated subcolumns resemble those in reality, in particular the vertical correlation relationship. Contrary to the scaling approach above, this method aims to resolve cloud geometry in a direct manner. The algorithm used to generate vertical correlation profiles is akin to that in cloud cover overlap but with a different decorrelation length L_{cw}(Raisanen et al., 2004). Hogan and Illingworth (2003) found L_{cw}typically varies between 0.5 and 2 km for a domain range of 2 to 300 km. Oreopoulos et al. (2012) fixed L_{cw}at 1 km and examined its impacts on radiative budgets in GEOS-5 (Goddard Earth Observing System Model, Version 5). These studies neglected the varying feature of L_{cw} in the vertical dimension; however, this was at the cost of accuracy, as will be shown later. The goal of this study was thus to propose a new parameterization of L_{cw} that accounts for vertically varying characteristics and to compare it with previous parameterizations.

This study, targeting cloud condensate vertical alignment, is a follow up to Wang et al. (2016), which focused on cloud cover overlap. The decorrelation length L_{cf} in Wang et al. (2016) is used to adjust the degree of cloud fraction overlap, while L_{cw}in this study is used to adjust cloud condensate vertical alignment. The paper is structured as follows. Section 2 details a new parameterization of L_{cw} based on cloud resolving model (CRM) simulations of two deep convective systems. Section 3 compares variousL_{cw}, including the new parameterization, in terms of simulated CRFs and radiative heating rates. Also explored in this section are reasons for the distinct behavior of different parameterizations and the role of L_{cw} in modulating these fields. Section 4 discusses the relative importance between cloud cover overlap and cloud condensate alignment. The last section summarizes the main findings of this study.

2. Diagnosis and parameterization of L_{cw}

2.1. Cloud condensate vertical alignment in CRM simulations

Cumulus clouds are usually associated with large subgrid horizontal variability because of intense turbulence inside the clouds (Wang et al., 2015). Fig. 1a shows the subgrid cloud water (liquid + ice) distribution for one snapshot simulation of deep convection by the SAM (System for Atmospheric Modeling) cloud-resolving model (Khairoutdinov and Randall, 2003). Technical details of the model configuration can be found in Wang et al. (2016). The subgrid in this study refers to the CRM grid at the resolution of 4 km, and any variability in the horizontal dimension is down to this scale. Fig. 1a indicates that cloudy cells are widely spread in the upper two layers (blue), whereas they are sporadically distributed in the middle layers (red). This is consistent with the fact that anvil clouds usually occupy a larger cloud fraction and convective cores occupy a smaller cloud fraction. A remarkable peak-to-peak correspondence is apparent between the two convective layers, even though they span as far as 3 km. However, such a clear correlation is not apparent in the two anvil layers, although they are adjacent to each other with an interval of <500 m. It is thus implied that vertical correlation and decorrelation length L_{cw}varies in different cloud regimes. Although the homogenous assumption excludes any variability at each level, variability remains in the cloud condensate path (CCP) (green line in Fig. 1b), which is also reflected in the cumulative condensate path (green line in Fig. 2b). It is important to remember the geometry of cloud hydrometeors is governed by that of cloud cover, in view of the fact that cloud hydrometeors can only exist within cloudy cells. Constrained by the same cloud cover geometry shown in Fig. 2a, the generated stochastic subcolumns under two L_{cw} extremes are shown in Fig. 1c and d. Details of the stochastic method will be provided in Section 3.1. We noticed that maximum overlap (MO,$L_{cw} = \infty$) produces higher peak-to-peak correlation, while random overlap (RO, $L_{cw} = 0$) generally weakens the correlation. As a result, the maximum value of CCP is increased under MO, whereas it is somewhat decreased under RO conditions.

2.2. Diagnosis of L_{cw}

First, to diagnose L_{cw} from CRM simulations, the correlation coefficient ρ is calculated for any two adjacent levels. Here, the correlation

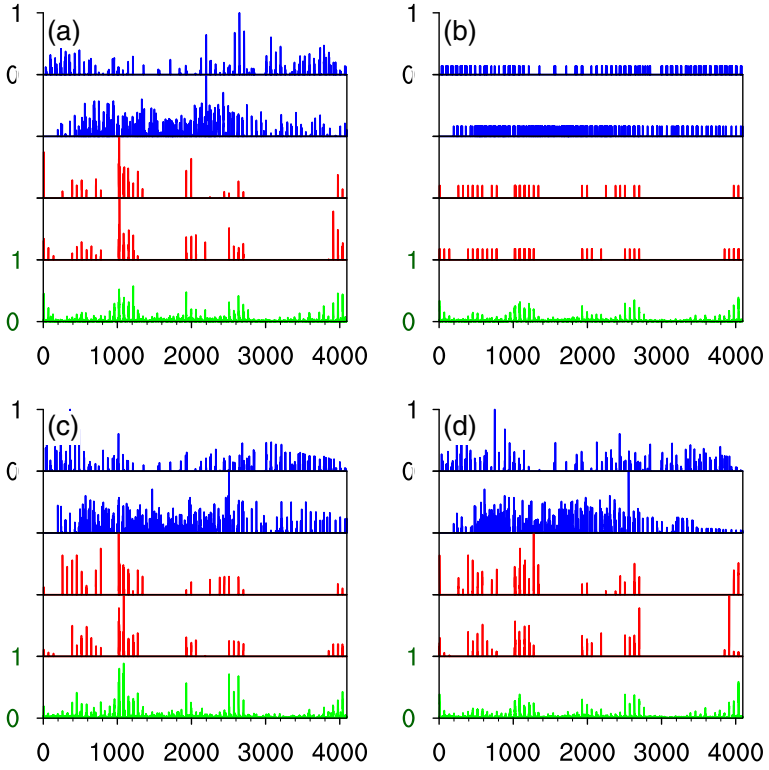

Fig. 1. Horizontal subgrid distribution and vertical alignment of cloud hydrometeors under (a) CRM output geometry, (b) PPH, (c) maximum overlap and (d) random overlap assumptions. The abscissa is the number index of CRM subcolumns and the ordinate is relative values of cloud hydrometeor amount (blue and red) and cloud condensate path (green).

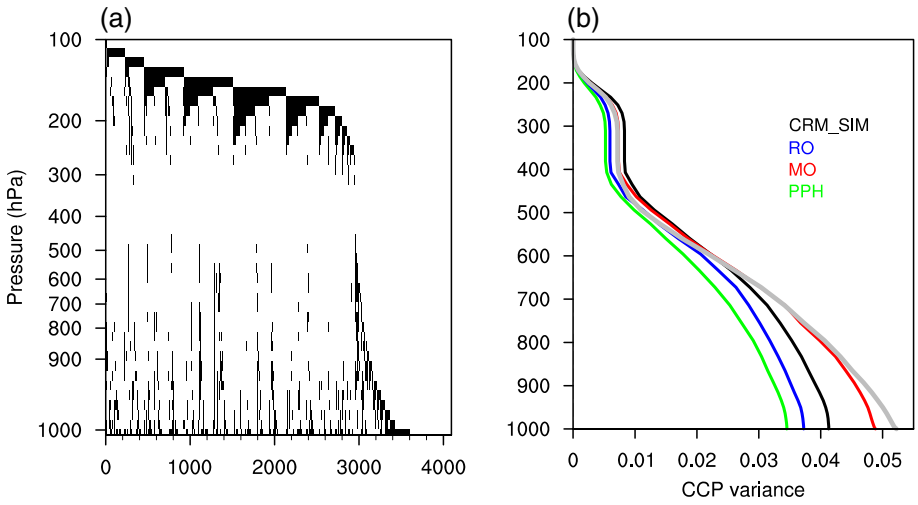

Fig. 2. (a) Binary maps of a two-dimensional cloud field reordered according to cloud-top height for one snapshot of CRM simulations. (b) Downward cumulative cloud condensate path variance. The abscissa in Fig. 2a is the number index of CRM subcolumns.

was based on the rank index of cloud hydrometeors following Raisanen et al. (2004), whereas Hogan and Illingworth (2003) chose to use the hydrometeor content in their studies. The rank index refers to the index order that is sorted from small to large according to values of cloud hydrometeor content. Next, L_{cw} was derived according to Eq. (1) by assuming the correlation drops off exponentially with vertical distance (Hogan and Illingworth, 2003):

$$\rho = \exp\left(-\int_{z_k}^{z_{k-1}} \frac{dz}{L_{cw}(z)}\right). \quad (1)$$

Fig. 3 displays the computed correlation coefficient ρ and corresponding L_{cw} for two deep convective cases. The first is the Tropical Rainfall Measuring Mission (TRMM) Kwajalein Experiment (KWAJEX), which was conducted around the Kwajalein Atoll in the Republic of the Marshall Islands (7–10°N, 166–169°E) in 1999. This case has been widely used in convection and cloud studies (e.g., Schumacher et al., 2008; Wang and Zhang, 2013). The second field campaign is the Global Atmospheric Research Program's Atlantic Tropical Experiment (GATE Phase III), which took place in the summer of 1974. More details about these two cases and the corresponding CRM simulations are described in Wang et al. (2016).

For both cases, high ρ values (>0.8) are preferentially observed within convective layers, implying the rank index of cloud condensates tends to be maximally overlapped. As a consequence, $L_{cw}$is large. Meanwhile, ρ is generally low (<0.5) in cirrus clouds, thereby corresponding to a smaller L_{cw} (<1 km). This demonstrates that parcels within convective regions are well organized and can keep the rank index even after ascending some distance, whereas cirrus clouds favor the random alignment, presumably due to chaotic turbulent processes.

2.3. Parameterization of L_{cw}

Fig. 4a presents the median value of L_{cw} and the inter-quartile range at each level for the KWAJEX and GATE cases. It is encouraging that the envelope of the inter-quartile range generally shows a similar behavior

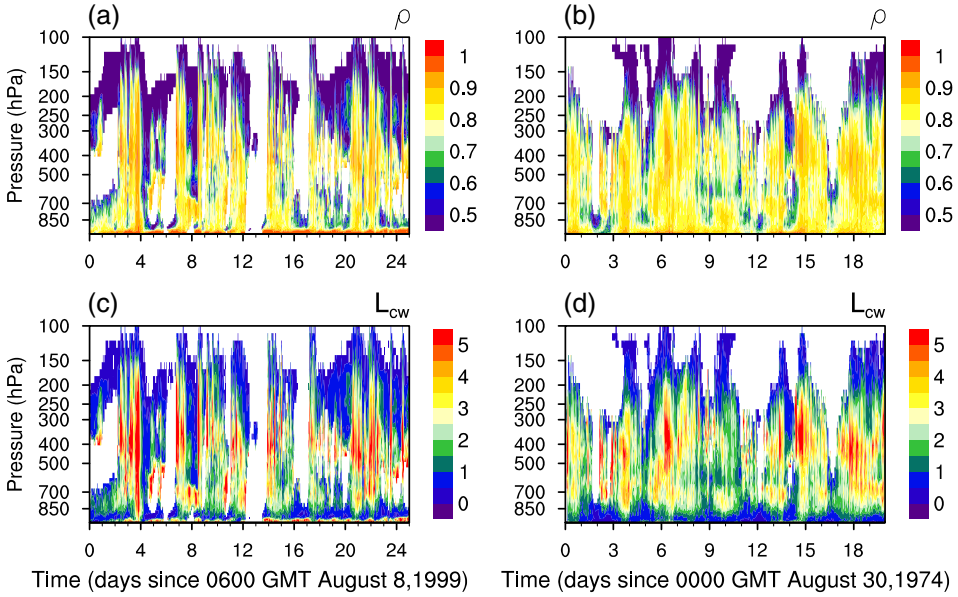

Fig. 3. Condensate correlation ρ (a, b) and decorrelation length L_{cw} (c, d) (units: km) diagnosed from CRM output cloud geometry for the KWAJEX case (a, c) and GATE case (b, d).

as the median L_{cw}, although the uncertainty can be as large as 1 km around 400 hPa. It is indicated that L_{cw} does not differ significantly between the two cases and can be well expressed by a piecewise function:

$$L_{cw} = \begin{cases} \max\left(0.5\ ,\ 2.3 + \dfrac{P-400}{250} \times 1.8\right) & P<400\,\text{hPa} \\ 2.3 & 400 \le P < 750\,\text{hPa} \\ \max\left(0.6\ ,\ 2.3 - \dfrac{P-750}{175} \times 1.7\right) & P \ge 750\,\text{hPa} \end{cases} \quad (2)$$

Using Eq. (2), the vertically varying characteristics of L_{cw} are now well captured (black line in Fig. 4a). Such a varying structure in L_{cw} is reminiscent of a similar structure in the cloud cover decorrelation lengthL_{cf}. To show this similarity, Fig. 4b presents a scatter plot of L_{cw} versus L_{cf}, which is diagnosed from the same dataset (Wang et al., 2016). Overall, a positive correlation was observed, in spite of considerable scatters. The larger L_{cf} corresponds to a largerL_{cw}, with the latter nearly halved by the former. Their relationship is linearly regressed as

$$L_{cw} = 0.65L_{cf} + 0.31. \quad (3)$$

By substituting the L_{cf} expression derived in Wang et al. (2016), the newly parameterized L_{cw} is superimposed in Fig. 4a (blue dashed line). It is clear that the results bear close resemblance to that using Eq. (2), corroborating the validity of Eq. (3).

3. Effects of cloud condensate vertical alignment on radiation

This section examines the effects of cloud condensate vertical alignment on radiative budgets and heating fields under variousL_{cw}, including the new parameterization described above. The main aim is to explore how radiative characteristics behave under different L_{cw} and the role of L_{cw} in modulating the cloud radiative transfer process.

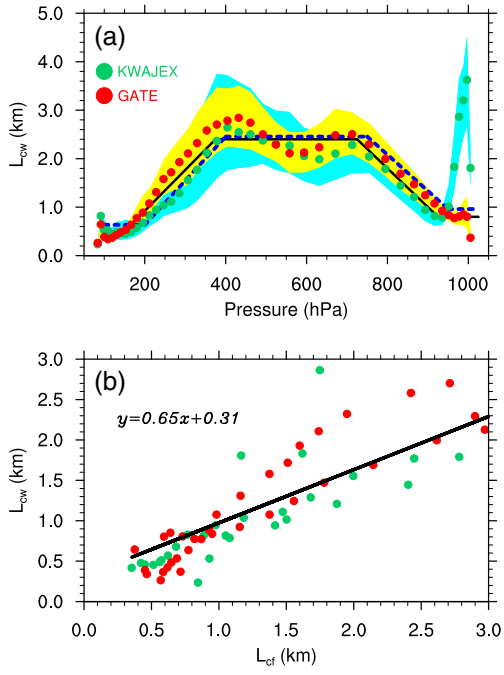

Fig. 4. (a) CRM diagnostic median L_{cw} for KWAJEX (green dots) and GATE (red dots) as a function of pressure. Cyan and yellow shading stands for inter-quartile ranges of L_{cw} for KWAJEX and GATE, respectively. (b) Scatter plot of L_{cw} versus L_{cf}. The black solid and blue dashed curves in (a) are for parameterizations according to Eqs. (8) and (9), respectively. The black line in (b) is the optimum linear function under least error analysis.

3.1. Model and experimental design

The radiative transfer model is a single column version of the Rapid Radiative Transfer Method for GCMs (RRTMG), which uses an efficient and accurate correlated-*k* method for calculating radiative fluxes and heating rates (Clough et al., 2005). In addition, a stochastic cloud generator is employed to generate stochastic subcolumns within large-scale model cells (Raisanen et al., 2004). The model was configured as follows: the surface albedo was set to 0.2 and the solar constant was set as 1367 W m^{-2}. A daily-averaged zenith angle of 71.8° was used, so that there was no diurnal cycle. One might question the averaged zenith used here, as in this case cloud effects on shortwave would be artificially prolonged. However, this was verified and the results indicated no systematic differences between simulations using daily-averaged and time-varying zeniths (see Fig. A1 in Appendix).

The treatment of cloud condensate vertical alignment is detailed below. Following Raisanen et al. (2004), the amount of cloud liquid/ice water $w_{j,k}$for one particular level *k* of each subcolumn *j* was determined according to the following equations:

$$R_{j,k} = \int_0^{w_{j,k}} p_{j,k}(w)dw, \quad (4)$$

$$R_{j,k} = \begin{cases} R_{j,k-1}, & random1_{j,k} \le \exp\left(-\int_{z_k}^{z_{k-1}} \dfrac{dz}{L_{cw}(z)}\right) \\ random2_{j,k}, & random1_{j,k} > \exp\left(-\int_{z_k}^{z_{k-1}} \dfrac{dz}{L_{cw}(z)}\right) \end{cases}, \quad (5)$$

where*w* represents cloud condensate, including both 'precipitating' and 'suspended' categories; $p(w)$ is a normalized probability density function for *w*; the subscript *j,k* denotes the layer where cloud occupies at subcolumn *j*; *z* is altitude; and $random1_{j,k}$ and $random2_{j,k}$ are random numbers distributed evenly between 0 and 1. To obtain the value of hydrometeor content at any level in a subcolumn, one can first use Eq. (5) to generate the cumulative frequency distribution (rank) of *w*, and then Eq. (4) to obtain *w* at a particular level if $p(w)$ is given. For the sake of simplicity, $p_{j,k}(w)$ was not parameterized but tabulated according to CRM output values in this study. In practice, the sampling strategy without replacement (i.e., all rank indexes should and must be traversed only once) is used to make sure cloud statistics in the horizontal dimension are exactly the same as in CRM while satisfying the ranking correlation constraint in the vertical dimension. To exclude influences from cloud cover overlap, the same cloud cover geometry from the CRM simulation was used. Thus, any discrimination in cloud radiative characteristics could only arise from the difference in cloud condensate vertical alignment.

The RRTMG model runs seven experiments in total: the CRM_SIM experiment using the CRM output cloud condensate geometry, and six sensitivity experiments, labeled as PPH for the plane parallel homogenous assumption, PPH_scaling for the run similar to PPH but multiplied with a scaling factor of 0.7, and RO (random overlap, $L_{cw} = 0$), MO (maximum overlap,$L_{cw} = \infty$), LO_1km ($L_{cw} = 1$ km), and LO_varied (Eq. (2)) for four overlap assumptions in line with different L_{cw}. For brevity, the details of these experiments are listed in Table 1.

3.2. Deficiency of the PPH assumption

Before examining the performance of stochastic ICA approach, the deficiency of traditional PPH assumption is highlighted. Fig. 5 shows the time series of SWCF (shortwave CRF) and LWCF (longwave CRF) biases against CRM_SIM. Both SWCF and LWCF are substantially overestimated, which is consistent with previous studies reporting that PPH would intensify cloud radiative effects (Carlin et al., 2002). The error is as large as −100 W m^{-2} for SWCF and 80 W m^{-2} for LWCF, which are offset between each other, yielding an error of −20 W m^{-2} for net CRF. The PPH scaling approach only brings limited

Table 1
Experiment descriptions.

Experiment name	Description
CRM_SIM	CRM output cloud condensate geometry
PPH	Plane-parallel homogenous assumption
PPH_scaling	PPH with a scaling factor of 0.7
RO	Radom overlap ($L_{cw}=0$)
MO	Maximum overlap ($L_{cw}=\infty$)
LO_1km	Moderate overlap ($L_{cw}=1$ km)
LO_varied	Varying L_{cw}in the vertical dimension

improvement, alleviating the overestimation by <10%. This demonstrates that the scaling factor of 0.7 originally derived from marine stratocumulus clouds is inappropriate for cumulus clouds. In fact, specifying proper scaling factors for different cloud types remains the greatest difficulty of the PPH scaling approach.

Why PPH always leads to overestimated CRFs? Following Shonk and Hogan (2008), the albedo α is written in terms of cloud optical depth τ as in Eq. (6). The relationship between emissivity ε and τ is approximately expressed as in Eq. (7), which is well satisfied under the zero-scattering approximation for longwave.

$$\alpha = 0.2 + 0.525\frac{\tau}{\tau + 3.5} \tag{6}$$

$$\varepsilon = 1 - \exp(-1.66\tau) \tag{7}$$

Graphical representations of the above relationships are shown in Fig. 6. For two arbitrary values of τ in shortwave (e.g., $\tau_1 = 2$, $\tau_2 = 25$), the average optical depth τ_{ave} equals 13.5, and this leads to an albedo $\alpha(\tau_{ave})$ of 0.617. However, the average albedo calculated by the average of $\alpha(\tau_1)$ and $\alpha(\tau_2)$ is 0.525. Thus, the PPH assumption gives an albedo in error by 17.5% and always leads to a larger α because of the convex relationship. The same analysis applies for emissivity ε as well, which is shown in Fig. 6(b). Therefore, it is the convex relationship between τ and α (ε) that essentially leads to an overestimation in $\alpha(\varepsilon)$.

3.3. Impacts of L_{cw} on CRF

This section evaluates the performance of stochastic ICA approach under different L_{cw}, with the goal to understand how L_{cw} influences cloud radiative budgets. The biases of domain-averaged SWCF and LWCF under RO, MO and LO_1km against CRM_SIM are shown in Fig. 7. In both cases, the overestimation of SWCF compared to CRM_SIM is remarkably reduced under LO_1km, almost to one third of that under PPH. Similar improvements are also apparent in LWCF, with the error being within the range of 20 W m^{-2}, in contrast to 80 W m^{-2} under PPH. The net CRF is also improved, with the error values between −15 and 10 W m^{-2}, in contrast to −30 W m^{-2} under PPH. By using a vertically varied L_{cw}expressed in Eq. (2) (LO_varied), the biases are further reduced, i.e., the overestimation is reduced by 8 W m^{-2} for SWCF and 2 W m^{-2} for LWCF in comparison with L_{cw} = 1 km (LO_1km) (see Fig. 8). Regarding the other two forms of L_{cw}, the overestimation of SWCF and LWCF is somewhat exaggerated under RO, whereas it is alleviated under MO though the sign is changed. The net CRF is thus positively biased under MO, as the SWCF is overly underestimated.

It is interesting to note that CRF decreases with increasing L_{cw}. This raises the question as to why increasing (decreasing) L_{cw}leads to decreased (increased) CRF. To physically interpret this, the radiative sensitivity of L_{cw} is approximately expressed as

$$\frac{\partial F}{\partial L_{cw}} \approx \frac{\partial F}{\partial \langle\tau\rangle}\frac{\partial \langle\tau\rangle}{\partial L_{cw}} + \frac{\partial F}{\partial \sigma_\tau}\frac{\partial \sigma_\tau}{\partial L_{cw}}, \tag{8}$$

where F is the net radiative flux at the atmosphere top, $\langle\tau\rangle$ denotes the mean cloud optical depth for the cloudy part, and σ_τ stands for the relative standard deviation of τ. Suppose cloud particle size is not a

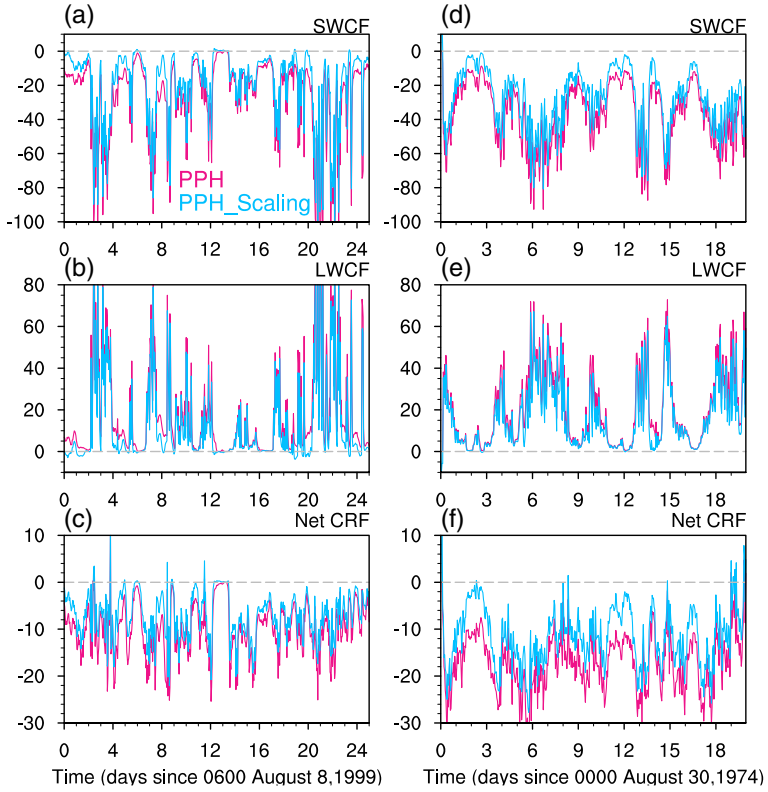

Fig. 5. CRF biases under PPH and PPH_scaling against CRM_SIM for the (a, b, c) KWAJEX case and (d, e, f) GATE case; (a, d) are shortwave CRF, (b, e) are longwave CRF, (c, f) are net CRF (units: W m^{-2}).

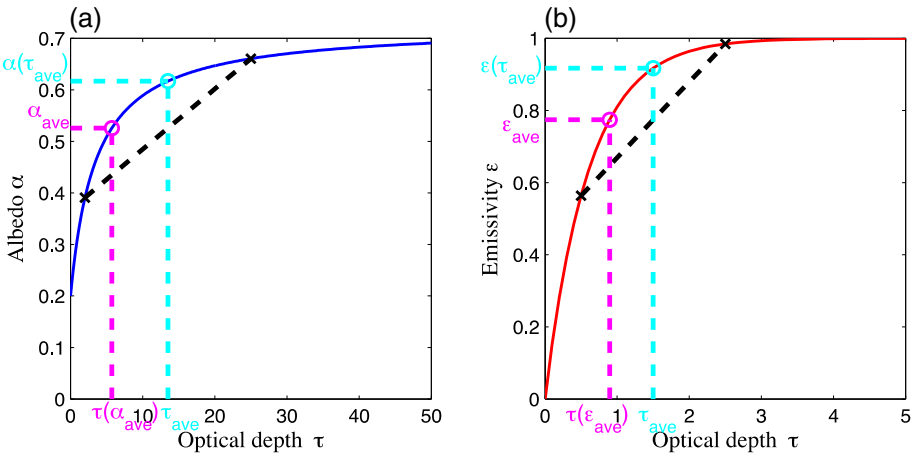

Fig. 6. (a) Solar albedo α and (b) thermal emissivity ε as a function of optical depth τ. The cyan circle denotes $\alpha(\varepsilon)$ at averaged τ, while the purple circle denotes averaged $\alpha(\varepsilon)$ at individual τ.

function of cloud condensate, modifications of L_{cw} thus do not alter$\langle\tau\rangle$. As such, the first term on the r.h.s of Eq. (8) can be omitted and Eq. (8) is then simplified as

$$\frac{\partial F}{\partial L_{cw}} \approx \frac{\partial F}{\partial \sigma_\tau}\frac{\partial \sigma_\tau}{\partial L_{cw}} \tag{9}$$

As illustrated in Section 3.2, $\frac{\partial F}{\partial \sigma_\tau}$is mainly subject to the convex relationship between τ and α (ε). $\frac{\partial \sigma_\tau}{\partial L_{cw}}$measures the effect of L_{cw}on σ_τ, which is primarily via modulating the variance of cloud water path. Fig. 9 shows the relative standard deviation of cloud water path under different L_{cw}. Apparently, MO produces the largest variance while RO yields the smallest. Between these lie the values generated by LO_1km and LO_varied, with the latter moderately larger than the former. The increased variance with increasing L_{cw} is obvious, as dense and tenuous parts of the cloud field would be increasingly aligned in the vertical dimension, thereby broadening $p(w)$ (Barker and Raisanen, 2005). This may cause confusion as to why LO_varied with optimal L_{cw} does not perform the best and why variances in MO do not always exceed those in CRM_SIM as one would expect. This is because the subcolumn optical depth τ depends not only on the rank index of cloud hydrometeors at each level, but also on the number of cloudy layers in the subcolumn. If dense parts of the cloud do not correspond to the subcolumn

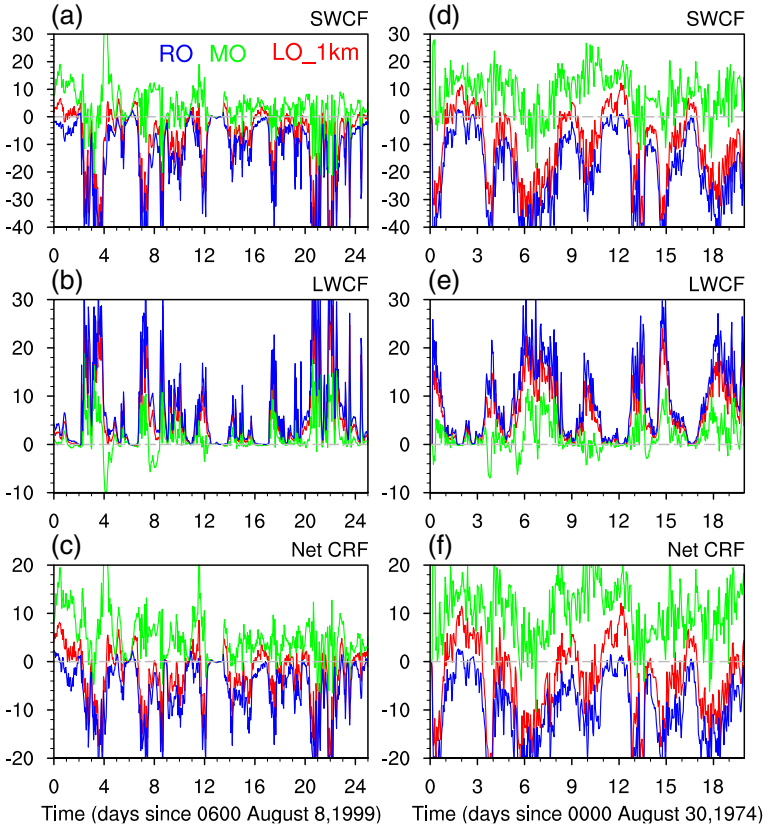

Fig. 7. CRF biases under RO ($L_{cw}\infty$), MO ($L_{cw}\infty$), and LO_1km (L_{cw}1 km) against CRM_SIM for the (a, b, c) KWAJEX case and (d, e, f) GATE case; (a, d) are shortwave CRF, (b, e) are longwave CRF, (c, f) are net CRF (units: W m^{-2}).

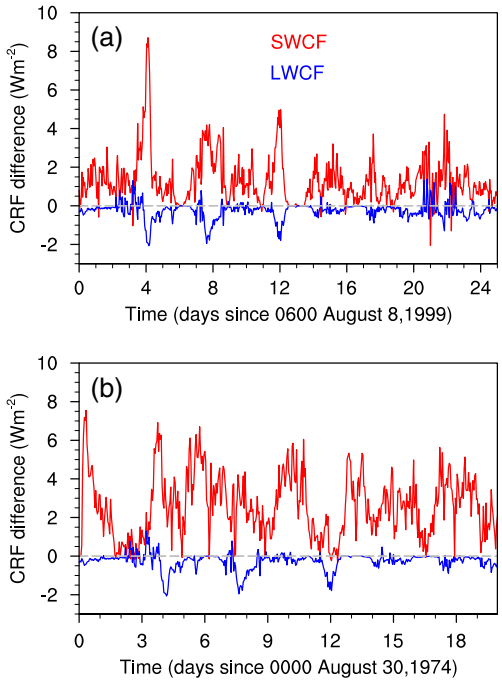

Fig. 8. CRF differences between LO_varied and LO_1km for the (a) KWAJEX case and (b) GATE case (units: W m^{-2}).

associated with thickest clouds, the peak of τ would be reduced and then cause a decrease in σ_τ. For instance, the gray line in Fig. 2b shows one possible profile by rotating the rank matrix. As is shown, an even larger σ_τ is obtained in the lower levels. In other words, MO does not necessarily guarantee a maximum $\sigma_\tau$among all possibilities. This also demonstrates that the effect caused by vertical alignment of cloud condensate is slaved to that of cloud cover.

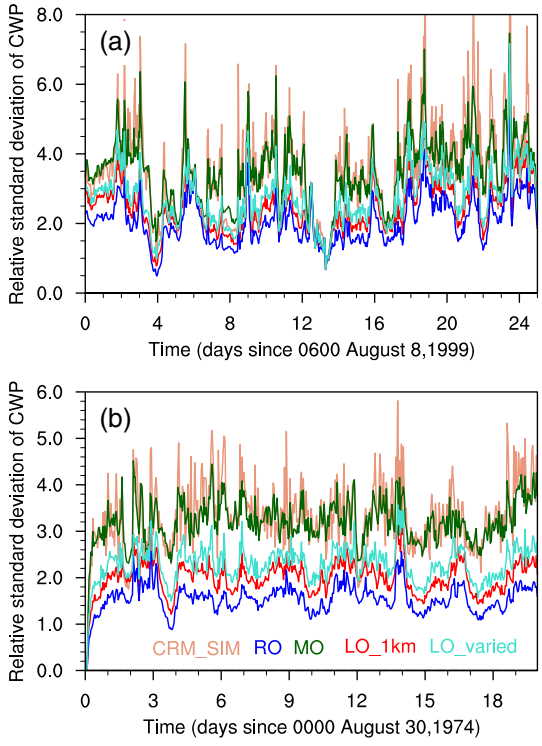

Fig. 9. Relative standard deviation of cloud water path under different overlap assumptions for the (a) KWAJEX case and (b) GATE case.

3.4. Impacts of L_{cw} on radiative heating

To determine how cloud condensate vertical alignment influences radiative heating, Fig. 10 gives the period-averaged bias of radiative heating under various L_{cw} against CRM_SIM. For shortwave heating, all simulations exhibit positive biases in upper layers and negative biases in lower layers. Among all, RO produces the largest errors, with the magnitude reaching as high as 0.2 K day^{-1}. The errors are markedly decreased in LO_1km and further reduced in LO_varied. Overall, MO performs the best, with the error almost reduced to one third of that in RO. With regards to longwave heating, the bias pattern is nearly out of phase to that of shortwave heating in the lower levels. The total heating is thereby less biased and closely resembles longwave heating (Fig. 10c and f).

As implied in Eq. (9), radiative flux and thus the heating are closely related to σ_τ. Fig. 11 presents the downward cumulative variance of CCP under different L_{cw}, with the CRM output value superimposed as a reference. In comparison with CRM_SIM, all simulations underestimate the variance of CCP at all levels. Among all, RO produces the largest errors while MO produces the smallest. As mentioned in Section 3.3, the cumulative optical depth τ depends not only on the rank index of cloud condensate, but also on the number of cloudy layers in the subcolumn. This also explains why LO_varied deviates from CRM_SIM even though more realistic L_{cw} is used. The advantage of vertically varied L_{cw} over $L_{cw} = 1$ km is prominent, as manifested in improved structures of cloud condensate variance and radiative heating.

4. Cloud cover overlap versus cloud condensate alignment

As cloud condensate alignment and cloud cover overlap have much in common in many aspects, this section uncovers their relative importance in modulating CRFs. Fig. 12 gives period-averaged CRF biases under different decorrelation lengths L_{cw} and L_{cf}. The CRF bias in line with different L_{cf} was studied in Wang et al. (2016) and is directly applied here. For either cloud cover or condensate, the random overlap leads to significant overestimations of CRFs in comparison with the CRM simulation. The bias magnitude caused by cloud cover is about twice to four times larger than that caused by cloud condensate, i.e., -50 W m^{-2} versus -13 W m^{-2} for SWCF, and 18 W m^{-2} versus 8 W m^{-2} for LWCF in the KWAJEX case. Though RO leads to considerable biases in both SWCF and LWCF, it is superior to the PPH approach (pink bars), which causes biases about twice as large as those of RO. The maximum overlap leads to significant underestimations of SWCF, i.e., 40 W m^{-2} by cloud cover versus 9 W m^{-2} by cloud condensate in the GATE case. With regards to LWCF, contrary to pronounced underestimations caused by cloud cover (i.e., -18 W m^{-2} for KWAJEX and -20 W m^{-2} for GATE), moderate overestimations (≤ 2 W m^{-2}) are produced when MO is applied in cloud condensate. By using a fixed L_{cw} of 1 km and L_{cf} of 2 km, both SWCF and LWCF are getting improved in comparison with RO, which leads to improved net CRFs as well, with the error <4 W m^{-2} for cloud condensate and 8 W m^{-2} for cloud cover. These biases are further reduced when the vertically varied L_{cw} or L_{cf} is used. In general, the uncertainty caused by cloud cover overlap can induce a CRF bias that is about twice to four times larger than that caused by cloud condensate alignment. Although cloud condensate alignment gives way to cloud cover overlap in regards to their impacts on CRFs, yet it still has enough of an effect in modulating CRFs as revealed above.

5. Concluding remarks

Diagnostic results based on CRM explicit simulations show that cloud condensate decorrelation length L_{cw} varies in the vertical dimension, with larger L_{cw} occurring in cumulus clouds and smaller L_{cw} in cirrus clouds. This means convective parcels can appropriately maintain the rank index even after ascending some distance, whereas a loss of the ranking order tends to occur in cirrus clouds. A new

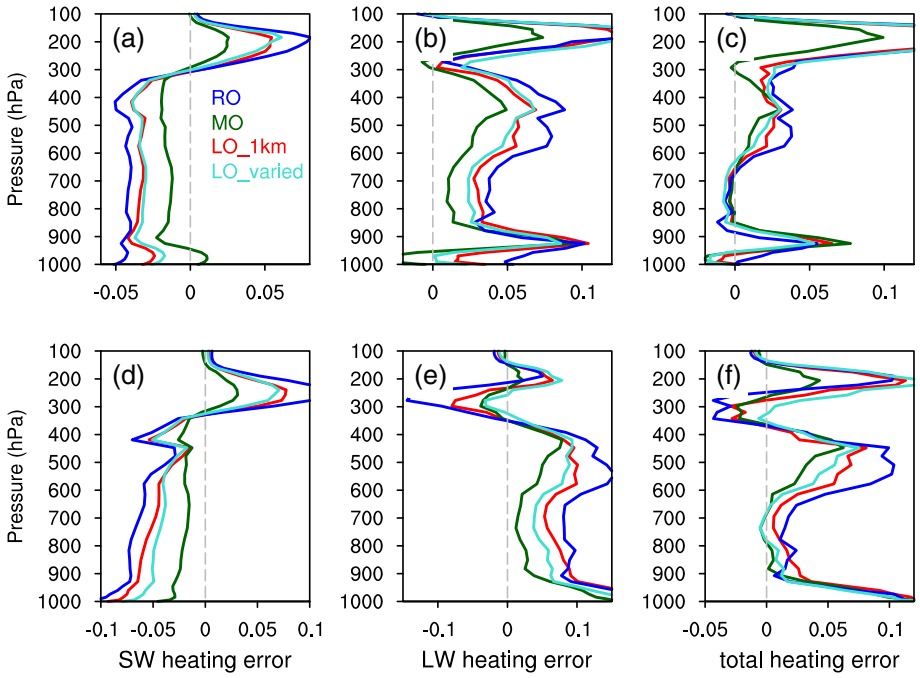

Fig. 10. Period-averaged biases of radiative heating rates for the (a, b, c) KWAJEX case and (d, e, f) GATE case; (a, d) are shortwave heating, (b, e) are longwave heating, and (c, f) are total radiative heating (units: K d^{-1}).

parameterization of L_{cw} that accounts for such varying characteristics is proposed, as opposed to the previous approach assumingL_{cw}unvaried in the vertical dimension. This new parameterization, though *ad hoc*, produces moderate improvements in simulations of CRF and radiative heating in contrast with $L_{cw} = 1$ km, i.e., the peak of bias is respectively reduced by 8 W m^{-2} for SWCF and 2 W m^{-2} for LWCF. The fact that cloud hydrometer typically varies in the vertical dimension implies that cloud water (ice) at each level has different contributions to the column integrated optical depth variance σ_τ, thus assuming $L_{cw}$to be vertically varied is more accurate and thereby leads to improved CRFs.

In a comparison among simulations of $L_{cw} = 0$ (RO), $L_{cw} = 1$ km and $L_{cw} = \infty$(MO), we found increasing (decreasing) L_{cw} leads to decreased (increased) CRF. The role of L_{cw} in modulating CRFs is twofold. On the one hand, larger L_{cw} tends to yield larger standard deviation of optical depth σ_τ, as dense and tenuous parts of the cloud field would be increasingly aligned in the vertical dimension, thereby broadening the probability distribution. On the other hand, larger σ_τ typically leads to a decrease in solar albedo and thermal emissivity, as implied by their convex relationship with τ. As a result, $\sigma_\tau$is larger in MO and smaller in RO in comparison with $L_{cw} = 1$ km. Accordingly, the overestimation of CRF is getting aggravated in RO, whereas alleviated in MO though the bias sign is changed. The vertical structure of σ_τ affects radiative heating as well. Owning to a better representation of downward cumulative variance of CCP, the heating is least biased under MO while most biased under RO.

The relative importance between cloud cover overlap and cloud condensate alignment reveals that the former could induce a net CRF bias that is about twice to four times larger than the latter. It is thus concluded cloud radiative effects are mainly subject to cloud cover overlap, however cloud condensate alignment still has enough of an effect in modulating the cloud radiative transfer process and cannot be ignored.

Supplementary data to this article can be found online at http://dx.doi.org/10.1016/j.atmosres.2016.11.014.

Acknowledgements

The author thanks the two anonymous reviewers for their constructive comments that helped to clarify and improve the paper. Thanks also go to Dr. Minghua Zhang for providing the KWAJEX forcing data, and Dr. Marat Khairoutdinov for making his cloud-resolving model available to us. This work was jointly supported by the National Natural Science Foundation of China (Grant Nos. 41530426, 91537108, 91437219,

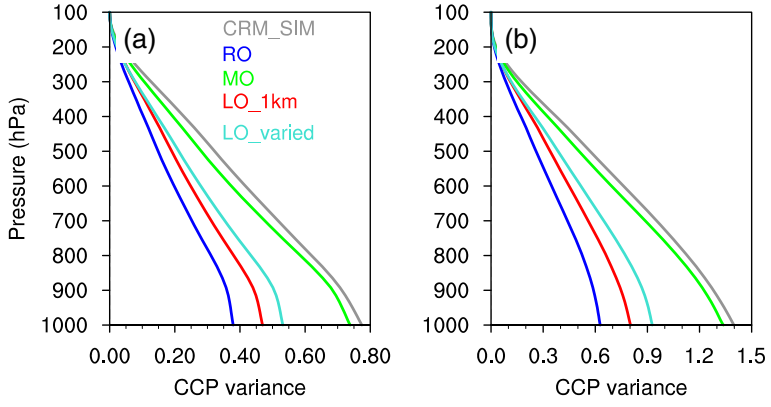

Fig. 11. Period-averaged simulations of downward cumulative CCP variances for the (a) KWAJEX case and (b) GATE case.

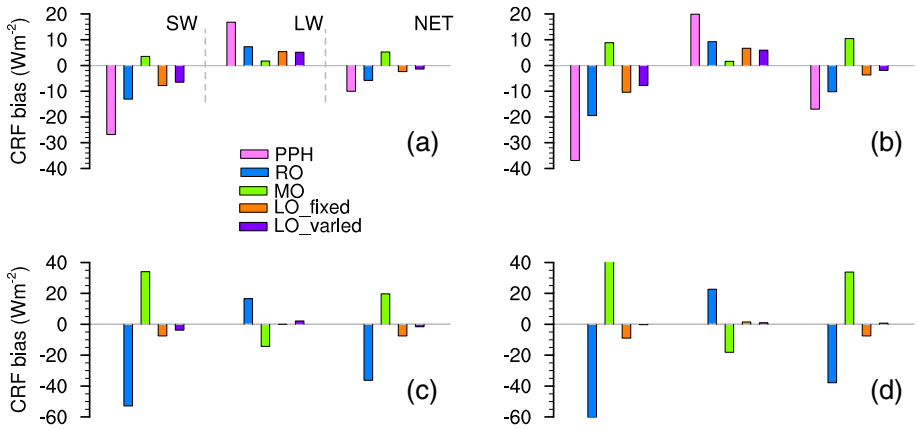

Fig. 12. Period-averaged CRF biases under different overlap assumptions for cloud hydrometeors (a, b) and cloud cover (c, d); (a, c) are for KWAJEX case and (b, d) are for GATE case.

41305102) and the Open Research Fund Program of Plateau Atmosphere and Environment Key Laboratory of Sichuan Province (Grant No. PAEKL-2016-K3).

References

Barker, H.W., Raisanen, P., 2005. Radiative sensitivities for cloud structural properties that are unresolved by conventional GCMs. Q. J. R. Meteorol. Soc. 131, 3103–3122.
Barker, H.W., Stephens, G.L., Fu, Q., 1999. The sensitivity of domain-averaged solar fluxes to assumptions about cloud geometry. Q. J. R. Meteorol. Soc. 125, 2127–2152.
Bony, S., Dufresne, J.L., 2005. Marine boundary layer clouds at the heart of tropical cloud feedback uncertainties in climate model. Geophys. Res. Lett. 32, 941–965.
Cahalan, R.F., Ridgeway, W., Wiscombe, W.J., Bell, T.L., Snider, J.B., 1994a. The albedo of fractal stratocumulus clouds. J. Atmos. Sci. 51, 2434–2455.
Cahalan, R.F., Ridgway, W., Wiscombe, W.J., Gollmer, S., Harshvardan, 1994b. Independent pixel and Monte Carlo estimates of stratocumulus albedo. J. Atmos. Sci. 51, 3776–3790.
Carlin, B., Fu, Q., Lohmann, U., Mace, G., Sassen, K., Comstock, J., 2002. High-cloud horizontal inhomogeneity and solar albedo bias. J. Clim. 15 (2421–2339).
Clough, S.A., Shephard, M.W., Mlawer, E.J., Delamere, J.S., Iacono, M.J., Cady-Pereira, K., Boukabara, S., Brown, P.D., 2005. Atmospheric radiative transfer modeling: a summary of the AER codes. J. Quant. Spectrosc. Radiat. Transf. 91, 233–244.
Gu, Y., Liou, K.N., 2006. Cirrus cloud horizontal and vertical inhomogeneity effects in a GCM. Meteorog. Atmos. Phys. 91, 223–235.
Hill, P.G., Hogan, R.J., Manners, J., Petch, J.C., 2012. Parameterizing the horizontal inhomogeneity of ice water content using CloudSat data products. Q. J. R. Meteorol. Soc. 138, 1784–1793.
Hogan, R.J., Illingworth, A.J., 2003. Parameterizing ice cloud inhomogeneity and the overlap of inhomogeneities using cloud radar data. J. Atmos. Sci. 60, 756–767.
Khairoutdinov, M.F., Randall, D.A., 2003. Cloud resolving modeling of the ARM summer 1997 IOP: model formulation, results, uncertainties, and sensitivities. J. Atmos. Sci. 60, 607–625.
Bogenschutz, P.A., Krueger, S.K., 2013. A simplified PDF parameterization of subgrid-scale clouds and turbulence for cloud-resolving models. J. Adv. Model. Earth. Syst. 5, 1–17.
Kuell, V., Bott, A., 2014. Stochastic parameterization of cloud processes. Atmos. Res. 143, 176–197.
Larson, V.E., Golaz, J.C., Jiang, H., Cotton, W.R., 2005. Supplying local microphysics parameterizations with information about subgrid variability: latin hypercube sampling. J. Atmos. Sci. 62, 4010–4026.
Lohmann, U., McFarlane, N., Levkov, L., Abdella, K., Albers, F., 1999. Comparing different cloud schemes of a single column model by using mesoscale forcing and nudging technique. J. Clim. 12, 438–461.
Oreopoulos, L., Lee, D., Sud, Y.C., Suarez, M.J., 2012. Radiative impacts of cloud heterogeneity and overlap in an atmospheric general circulation model. Atmos. Chem. Phys. 12, 9097–9111.
Pomroy, H.R., Illingworth, A.J., 2000. Ice cloud inhomogeneity: quantifying bias in emissivity from radar observations. Geophys. Res. Lett. 27, 2101–2104.
Raisanen, P., Barker, H.W., Khairoutdinov, M., Li, J.N., Randall, D.A., 2004. Stochastic generation of subgrid-scale cloudy columns for large-scale models. Q. J. Roy. Meteorol. Soc. 130, 2047–2067.
Schumacher, C., Ciesielski, P.E., Zhang, M., 2008. Tropical cloud heating profiles: analysis from KWAJEX. Mon. Weather Rev. 136, 4289–4300.
Shonk, J.K.P., Hogan, R.J., 2008. Tripleclouds: An efficient method for representing cloud inhomogeneity in 1D radiation schemes by using three regions at each height. J. Clim. 21, 2352–2370.
Tompkins, A.M., 2002. A prognostic parameterization for the subgrid-scale variability of water vapor and clouds in large-scale models and its use to diagnose cloud cover. J. Atmos. Sci. 59, 1917–1942.
Wang, X.C., Zhang, M., 2013. An analysis of parameterization interactions and sensitivity of single-column model simulations to convection schemes in CAM4 and CAM5. J. Geophys. Res. 118, 1–12.
Wang, X.C., Liu, Y.M., Bao, Q., Wu, G.X., 2015. Comparisons of GCM cloud cover parameterizations with cloud-resolving model explicit simulations. Sci. China Earth Sci. 58, 604–614.
Wang, X.C., Liu, Y.M., Bao, Q., 2016. Impacts of cloud overlap assumptions on radiative budgets and heating fields in convective regions. Atmos. Res. 167, 89–99.
Zhang, F., Liang, X.-Z., Li, J., Zeng, Q., 2013. Dominant roles of subgrid-scale cloud structures in model diversity of cloud radiative effects. J. Geophys. Res. 118, 7733–7749.